

Contents lists available at ScienceDirect

Chemical Engineering Journal

journal homepage: www.elsevier.com/locate/cej





In situ immobilization of δ -MnO₂ nanosheets on a porous support for rapid and continuous cleaning of bisphenol A-spiked water

Yu-Heng Deng a , Jemin Jeon a , Eun Mi Kim a , Shengzhe Ding a , Sang Ah Lee b , Changseon Ryu b , Young Jun Kim b , Xiao Su a , Hyunjoon Kong a,c,d,e,f,g,*

- ^a Department of Chemical and Biomolecular Engineering, University of Illinois at Urbana-Champaign, Urbana, IL 61801, United States
- ^b Environmental Safety Group, Korea Institute of Science and Technology (KIST) Europe, 66123 Saarbrücken, Germany
- E Department of Bioengineering, University of Illinois at Urbana-Champaign, Urbana, IL 61801, United States
- ^d Beckman Institute, University of Illinois at Urbana-Champaign, Urbana, IL 61801, United States
- e Carle Illinois College of Medicine, University of Illinois at Urbana-Champaign, Urbana, IL 61801, United States
- f Carl R. Woese Institute for Genomic Biology, University of Illinois at Urbana-Champaign, Urbana, IL 61801, United States
- g KU-KIST Graduate School of Converging Science and Technology, Korea University, Seongbuk-gu, Seoul 02841, South Korea

ARTICLE INFO

$\begin{tabular}{ll} Keywords: \\ BPA \\ EDC \\ Diatom \\ Polydopamine \\ MnO_2 \\ \end{tabular}$

ABSTRACT

Bisphenol A (BPA), a building block of various plastics, is invading biosystems through drinking water and raising concerns about their adverse impacts on human health. Filtration, biological, and oxidation methods have been developed to decontaminate BPA, but high energy demand or lengthy biodegradation process acts as limiting factors. Recently, δ-MnO₂ with layered structure has emerged as a promising tool for BPA degradation. However, the reaction rate of BPA degradation suffers from the nature of aggregation in free-standing δ -MnO₂ nanosheets with limited accessible active sites towards BPA. To overcome this critical challenge, this study demonstrates that the immobilization of δ-MnO₂ nanosheets on a porous support can enhance BPA degradation rate due to the increased exposure of active sites of δ -MnO₂. As a result, the δ -MnO₂ nanosheets immobilized on porous diatom particles via polydopamine (PDA) binder degrades BPA (k' ~0.774 L g⁻¹ min⁻¹) 14 times faster than free-standing δ -MnO₂ ($k' \sim 0.056 \text{ L g}^{-1} \text{ min}^{-1}$). Furthermore, the resulting δ -MnO₂-PDA-diatom degrades 99 % of BPA within 20 min and can be recycled without any performance loss up to 7 times, providing the reusability towards BPA removal in a sustainable and eco-friendly manner. More importantly, the degraded products of BPA resulting from radical transfers, coupling, and fragmentation reactions do not cause any estrogenic response or toxicity to ecological systems, as examined with human and fish cells. Finally, a column packed with δ-MnO₂-PDA-diatom demonstrates 99 % BPA removal with continuous flows of BPA-spiked wastewater. We propose that this advanced system will be readily extended to remove a broad array of water contaminants that will disrupt the physiological function of organs and their roles in the endocrine cross-talk between the reproductive hormones.

1. Introduction

Bisphenol A (BPA) is a building block of epoxy resins for dental sealants and food container lining [1–3]. Most BPA produced worldwide has also been used to synthesize polycarbonate plastics for food and beverage containers [4–7]. There is mounting evidence that BPA can leach from plastic containers and seep into food or beverages, which is the main route of BPA exposure to humans [8–10]. In addition, BPA released from plastic wastes can enter and accumulate in freshwater resources due to the incomplete removal of BPA by wastewater

treatment plants (WWTPs) and sewage treatment plants (STPs) [11–14]. As a result, BPA can be passed by the drinking water treatment plants (DWTPs), and enter the human body through water consumption [15–18]. Recent studies conducted with urine samples from volunteers in 50 different countries reported that BPA levels in human bodies are at least larger than 5 ng/kg [19]. Then, BPA breaches metabolites and causes adverse cardiovascular, reproductive, endocrine, and metabolic effects [20–23]. Therefore, developing targeted and efficient methods for remediation of BPA, and the mitigation of its contamination in the water cycle is imperative to secure human health.

^{*} Corresponding author at: Department of Chemical and Biomolecular Engineering, University of Illinois at Urbana-Champaign, Urbana, IL 61801, United States. E-mail address: hjkong06@illinois.edu (H. Kong).

Significant efforts have been made to develop tools and processes that can remove BPA from wastewater systems, including membrane separation [24–26], advanced oxidation processes (AOPs) [27–29], and biodegradation [30–32]. However, these treatment processes face challenges when operating on a large scale [33]. For instance, membrane separation needs to be used at high-pressure conditions reaching 30 bar [24]. AOPs usually require high-energy inputs such as ozone and ultraviolet light. Biodegradation using microorganisms can degrade BPA, but the slow degradation rates (*i.e.*, 1–3 days) and specific condition requirements for microbial cell growth act as limiting factors. Therefore, there are significant needs for a fast and energy-efficient BPA removal process.

Manganese dioxide (MnO₂) has emerged as a promising compound for BPA removal because of its robust oxidation capacity to degrade BPA through a series of radical reactions [34–36]. MnO₂ presents a variety of phase structures in nature (α -, β -, γ -, δ -, λ -MnO₂), all of which exhibit oxidative reactivity to degrade BPA [37–39]. In particular, δ -MnO₂ has the highest BPA degradation rate due to its high surface Mn (III) content and layered structure [37,40–42]. The Mn (III) on the surface possesses an anti-bonding electron readily being donated [37]. The layered structure provides more accessible active sites for the oxidation reaction than the tunnel-structured MnO₂ (e.g. α -, β -MnO₂) [42].

For efficient BPA degradation, it is desirable to immobilize $\delta\text{-MnO}_2$ on a support that can retain the active sites. Supported MnO_2 can prevent aggregation during the synthesis, thus leading to a higher number of active sites than free-standing MnO_2 [43,44]. In addition, the support can provide mechanical stability for ease of separation and recycling from heterogeneous reaction systems (i.e., gas- or liquid–solid reactions) [45]. However, the potential merits of the $\delta\text{-MnO}_2$ support have yet to be examined for BPA degradation, whereas most efforts are being made to uncover the BPA degradation mechanism.

To this end, this study demonstrates a strategy that fabricates δ-MnO₂ nanosheets in stable mechanical supports and, in turn, increases the BPA removal rate by one order of magnitude compared with freestanding δ-MnO₂ (Scheme 1). We hypothesized that immobilizing δ-MnO₂ nanosheets on a porous and robust micro-sized support using a polydopamine binder would increase active sites and, in turn, accelerate the BPA degradation in both water reservoir and continuous flow. To examine this hypothesis, first, we fabricated the δ -MnO₂ nanosheets on diatom biosilica particles using polydopamine (PDA) glue. Second, we assessed the extent to which the resulting δ -MnO₂-PDA-diatoms degrade BPA in terms of rate, yield, and recyclability. The free-standing δ-MnO₂ nanosheets were used as a control. In parallel, we analyzed the products resulting from the BPA degradation to address the mechanism by which δ-MnO₂-PDA-diatoms degrade BPA. Next, we further evaluated estrogenic activity, oxidative stress, and morphogenesis of human embryonic kidney cells and trout gill cells exposed to BPA-spiked water before and after treatment with δ-MnO₂-PDA-diatoms. Finally, we loaded the δ-MnO₂-PDA-diatoms into a packed bed column and examined their applicability to BPA removal in a continuous wastewater flow system.

2. Materials and methods

2.1. Fabrication of δ-MnO₂-PDA-diatom

Firstly, 1 g of diatom particles (diatomaceous earth-food grade, amorphous silica from freshwater type) were washed with deionized water and collected by centrifugation for 3 min at 1,000 rpm to remove impurities, repeating for 3 times. Then, the particles were resuspended in 320 mL of deionized water containing 0.8 g of dopamine hydrochloride (Sigma-Aldrich) under the stirring condition at 500 rpm. After 1 h, 80 mL of tris buffer solution (50 mM, pH = 8.5) was added to initiate polymerization of dopamine. The reaction was kept under the stirring condition at 500 rpm at room temperature overnight. The diatom particles coated with polydopamine (denoted as PDA-diatom) were collected using centrifugation at 1,000 rpm for 3 min and washed with deionized water 6 times. The PDA-diatoms were then dried in an oven at 60 °C for 2 days. The resulting dried powders of PDA-diatom were added in a 100 mM KMnO₄ (Sigma-Aldrich) solution with a mass/volume ratio of 10 (g L⁻¹) for 3 h. Finally, the particles (denoted as δ-MnO₂-PDAdiatom) were collected by centrifugation at 1,000 rpm for 3 min and washed with deionized water for 6 times. The δ-MnO₂-PDA-diatoms were then dried in an oven at 60 °C for 2 days and then stored in a vial for the following experiments.

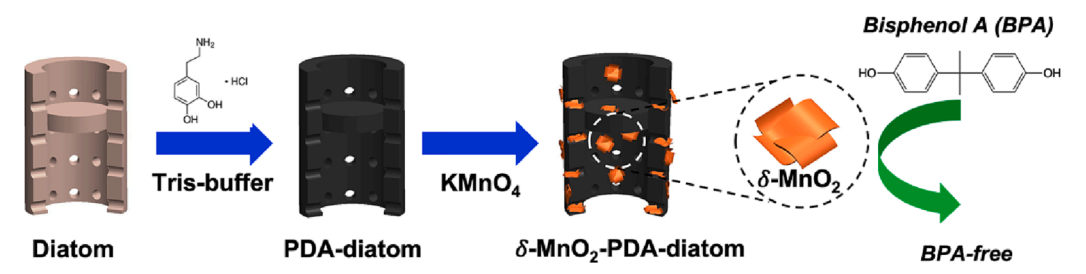
2.2. Characterizations of δ -MnO₂-PDA-diatom

The morphology and surface element mapping of particles were obtained using scanning electron microscope (SEM, FEI Quanta FEG 450) at 5 kV and energy dispersive spectroscopy (EDS, Hitachi S-4800) at 20 kV. The microstructures of particles were observed using transmission electron microscope (TEM, JEOL 2100) at an accelerating voltage of 200 kV. The manganese loading amount within δ -MnO₂-PDAdiatoms was measured by inductively coupled plasma mass spectrometry (ICP-MS, NexION 350D). The surface of MnO2-PDA-diatoms was analyzed by X-ray photoelectron spectroscopy (XPS, Kratos Axis ULTRA). The nitrogen adsorption/desorption isotherms of particles were analyzed using Micrometritics 3Flex Analyzer. The specific surface area of particles was calculated by Brunauere - Emmette - Teller (BET) equation with the obtained adsorbed nitrogen quantity within the relative pressure (P/P_0) range of 0.05 - 0.30. The pore volume and pore size of particles were calculated by Barrett - Joyner - Halenda (BJH) method with the obtained adsorbed nitrogen quantity within the relative pressure (P/P_0) range of 0.05 - 0.99. The crystallinity of particles was measured using X-ray diffraction (XRD, Rigaku MiniFlex 600) with Cu K α radiation ($\lambda = 0.154056$ nm) at a beam voltage of 40 kV and a beam current of 15 mA. The XRD pattern was obtained by scanning over the 2θ of $10^{\circ} - 70^{\circ}$ with a step size of 0.02° and a speed of 10° min⁻¹.

2.3. Fabrication of free-standing δ -MnO₂

Firstly, 1.9~g of KMnO₄ was dissolved in 30 mL deionized water. Separately, 6.72~g of potassium hydroxide (KOH, Sigma-Aldrich) was

Immobilization of δ -MnO₂ on porous support (diatom)



Scheme 1. Schematic illustrating immobilization of δ -MnO₂ nanosheets on porous support (diatom biosilica) for BPA removal.

dissolved in 18.4 mL ethanol and 21.6 mL deionized water [46]. Then, the KOH mixture was dropwise added to the KMnO₄ solution, followed by continuous stirring at 500 rpm for 1 h at ambient temperature. The mixture was subsequently heated at 80 °C to form $\delta\text{-MnO}_2$. After 48 h, the product was washed with water for 5 times and dried at 60 °C in an oven overnight.

2.4. BPA removal using δ -MnO₂-PDA-diatom and free-standing δ -MnO₂

All BPA removal tests were conducted in a 20-mL vial under. The stock BPA solution (44 µM) was prepared by dissolving BPA (Sigma-Aldrich) in distilled water using sonication for 2 h. The buffer solution was prepared with 25 mM acetate buffer at pH 5.0 and the ionic strength of the buffer solution was maintained with 0.01 M sodium chloride (Sigma-Aldrich). To initiate the reaction, an appropriate number of δ-MnO₂-PDA-diatoms or free-standing δ-MnO₂ was suspended in 9 mL of the buffer solution, followed by adding 1 mL of BPA stock solution. The BPA-containing mixture was stirred continuously at 500 rpm using a Teflon-coated stir bar. The temperature was kept constant at room temperature. Then, 1 mL of the mixture was collected at a designated time. The reaction between BPA and δ-MnO₂-PDA-diatoms was quenched with ascorbic acid (Sigma-Aldrich) solution. The δ-MnO₂-PDA-diatoms were separated from the solution using centrifugation at 15,000 rpm for 3 min. The supernatant was diluted with deionized water at a 1:1 vol ratio for HPLC analysis. The recyclability of δ-MnO₂-PDAdiatoms was conducted by repeatedly following the method mentioned above. For selectivity test, 2-chlorophenol was added into BPA stock solution and followed the same procedure above.

2.5. HPLC analysis of BPA concentration

The BPA degradation was quantified by a reversed-phase high pressure liquid chromatography (HPLC) (Agilent 1260 Infinity II, Agilent Technologies, USA; coupled with 1260 Infinity II Variable Wavelength Detector). Agilent Infinity Lab Poroshell 120 EC-C18 column (4.6 X 150 mm, 2.7 μm particle size) was used to separate BPA from reaction solutions with an isocratic mobile phase of 60% water and 40% acetonitrile (both in HPLC grade) at 20 °C and 0.5 mL/min. The injection volume was 60 μL . The retention time of BPA detected at 230 nm was 10.1 min under this condition. Both standards and experimental samples were prepared by adding one equivalent of DI water. The BPA concentration after the treatment was calculated based on a calibration curve.

2.6. LC-ESI/MS analysis of BPA-derived products after degradation

The products from BPA degradation by $\delta\text{-MnO}_2\text{-PDA-diatom}$ was identified by ultra-performance liquid chromatography-mass spectrometry (UPLC-ESI/MS) (Acquity UPLC 1- Class, Waters, USA; coupled with SYNAPT G2-Si Mass Spectrometer). The chromatographic separation was achieved by Waters Acquity HSS T3 C18 (2.1 X 50 mm, 1.6 μm particle size). The mobile phase was water (A) and acetonitrile (B) (both in HPLC grade) in gradient mode: 0–0.5 min from 30% B to 30% B, 0.5–5.0 min from 30% B to 95% B, 5.0–8.0 min from 95% B to 95% B, 8.0–8.1 min from 95% B to 30% B, and 8.1–10.0 min from 30% B to 30% B (v/v). The MS detector was operated in negative electrospray ionization (ESI) mode at full scan. The injection volume was 5 μL .

2.7. Transfection of estrogenic receptor expression in human embryonic kidney 293 (HEK293) cell line

The HEK293 cells were transduced with the pGreenFire Lentireporter plasmid (pGF2-ERE-rFLuc-T2A-GFP-mPGK-Puro; TR455VA-P, System Biosciences, USA) that encodes GFP reporter and red-shifted luciferase under the control of estrogen response element (ERE) with the puromycin resistance as per the previously developed method [47]. Briefly, the cells were plated at a density 3×10^5 cells per well in a 6-

well plate (145380, Thermo Scientific, USA) before transduction (n = 3). After overnight incubation at a 37°C chamber with 5.0% of CO₂, the medium was aspirated, and the virus-containing medium was treated with 5 $\mu g/mL$ of polybrene for eight hours. Subsequently, the virus-containing medium was removed, and the transduced cells were allowed to recover overnight before the addition of puromycin (10 $\mu g/mL$) for a selection.

The transduced cells (HEK293-ERE) were transfected with the piggyBac transposon gene expression system. The zER α expression vector was custom-cloned from the vector builder (pPB-Neo-CAG > zER α , VB210426-1022cns, Vectorbuilder Inc., USA), and the pRP-mCherry-CAG > hyPBase plasmid (VB160216-10057, Vectorbuilder Inc., USA) encodes the hyperactive version of piggyBac transposase. The cells were plated at a concentration of 1×10^5 cells per well in a 6-well plate and incubated overnight as specified before. The 1 μg of vector was mixed with 0.75 μL of Lipofectamine 3000 reagent in 250 μL of Opti-MEM medium and incubated for 15 min to allow for the formation of a DNA-lipid complex. Next, the complex was transferred to the wells and incubated for six hours. Then, the medium was removed, and the cells were allowed to recover overnight before adding puromycin and neomycin (10 $\mu g/mL$ and 2 $\mu g/mL$). Finally, the transfected cells (HEK293-ERE-zER α) were collected.

2.8. Estrogenic activities evaluation

Estrogenic activities induced by BPA was assessed with HEK293-ERE-zER α cells. Each well in a 96-well plate housed 1.0 \times 10⁴ cells with puromycin and neomycin (1 μ L/mL and 0.2 μ L/mL) (n = 7) before the incubation for 24 h at 37°C and 5% CO₂. 17 β -estradiol (E2), a selective estrogen receptor agonist, was used as a reference (positive control) at concentrations ranging from 9.52 \times 10⁻⁹ to 3 \times 10⁻⁶ mg/mL. BPA were prepared in half-logarithmic (3.16-fold) dilution in the acetate buffer resulting in the following concentrations from 3.17 \times 10⁻⁶ to 1 \times 10⁻³ mg/mL. In parallel, the treated-BPA solution was prepared by incubating BPA solution with 0.5 g/L or 1.0 g/L of δ -MnO₂-PDA-diatoms for 20 min, followed by filtration to remove the particles.

After 24 h of incubation at 37°C (5% CO₂), the growth medium was aspirated, and the cells were rinsed with 1X PBS (pH 7.4). The Passive Lysis Buffer (E194A, Promega, Germany) was added to each well by 20 μL and gently mixed for 10 min. The lysates were applied for evaluating luciferase activities by the Luciferase Reporter Assay System (E151A, Promega, Germany) according to the manufacturer's manual. The activities were measured as a relative luminescence unit with the 3 s integration time and 1 s settling time on a TECAN microplate reader (TECAN, Männedorf, Switzerland). The estrogenic response was calculated from the percentage induction against E2 (Equation (1)):

$$I(\%) = \left(OD_{570,s} - OD_{570,d}\right) / \left(OD_{570,E2} - OD_{570,d}\right) \times 100 \tag{1}$$

where I is percentage induction; $OD_{570,s}$ is the absorbance of the sample exposed to DBPs at 570 nm; $OD_{570,d}$ is the absorbance of the sample exposed to acetate buffer (control) without δ -MnO₂-PDA-diatom at 570 nm; $OD_{570,E2}$ is the maximally induced absorbance by E2.

2.9. Intracellular oxidative stress level measurement in RTgill-W1 cells

RTgill-W1 (ATCC CRL-2523) cells were cultured by following the manufacturer's instruction. After cell culture reached 80% confluency, the cells were harvested and resuspended in the culture media (Leibovitz's L-15, ATCC) containing 10% fetal bovine serum and 1% penicillin/ streptomycin. The cell suspension was further inoculated in a glass-bottom petri-dish with a density of 10,000 cells cm $^{-2}$. After 24 h incubation at 20 °C, the media was removed and replaced with new media or media containing BPA or BPA treated by $\delta\text{-MnO}_2\text{-PDA-diatoms}$. The media containing BPA (4.4 μM) was prepared by mixing the media with BPA (44 μM) acetate buffer-based solution at a ratio of 9:1

(v/v). For the media containing treated BPA, the BPA solution (4.4 μ M) was pre-treated with 1 g/L of δ-MnO₂-PDA-diatoms at 25 mM acetate buffer (pH = 5) for 2 h and then the solution was separated from particles by centrifugation and mixed with the media at 1:9 (v/v) ratio. The media for each condition was changed every day. After 5 days, the media was removed. 1 mL of CellROXTM reagent (Invitrogen, 10 μM) was added into the petri-dish for 30 min incubation. The media with Cell-ROXTM reagent was then removed and the cells were washed with PBS for 3 times. Thereafter, the cells were fixed by a mixture of acetone/ methanol (1:1) for 15 min, followed by DAPI (100 nM) staining for 5 min. The cells were preserved in PBS for confocal laser scanning microscope (Zeiss LSM 700) imaging. The images were taken using a 20x/ 0.8 air objective with line averaging of 4 and pixel dwell time of $6.30~\mu s$. Images acquisition and process were obtained through the Zeiss Zen software (Black and Blue, respectively). The intensity within a cell was measured using ImageJ software.

2.10. The morphology and permeability analysis of RTgill-W1 cells

The RTgill-W1 cells were cultured in culture media without BPA, media with BPA (10 $\mu g \; L^{\text{-}1}$), or media with BPA treated with $\delta\text{-MnO}_2\text{-PDA-diatoms}$ for 30 min. The culture was continued for 7 days. Separately, the collagen-based hydrogel utilized for the fish gill model was prepared as previously described [48]. Briefly, bovine type 1 collagen (Advanced Biomatrix) and polyethylene glycol were mixed at 1:4 mass ratio. Reconstitution solution (0.26 M sodium hydrogen carbonate, 0.2 M HEPES, and 0.04 M sodium hydroxide) was added to initiate gel formation via pH modulation. The solution was then incubated at 37 °C for 30 min. Then, RTgill-W1 cells were planted on the collagen-PEG hydrogel with 200,000 cells cm $^{-2}$ and cultured for 3 days to form the hollow fish gill-like lumen. The morphology of RTgill-W1 cells after 3 days was observed by a phase-contrast microscope (Leica DMIL).

In parallel, the F-actin within the cells was stained with fluorescent molecules for cellular structure observation. Firstly, the RTgill-W1 cells after exposed to BPA or BPA treated solution were fixed by 4% *para*-formaldehyde solution for 15 min. Then, the fixed cells were incubated with Alexa Fluor™ 594 phalloidin (Invitrogen) diluted 1:100 in blocking buffer (5% fetal bovine serum, 0.1% Tween-20 in PBS) for 1 hr at room temperature and counter-stained with DAPI (1:1000 dilution in blocking buffer). The resulting fluorescence-tagged cells were visualized by confocal laser scanning microscope (Zeiss LSM 700).

The permeability of RTgill-W1 cells treated BPA or $\delta\text{-MnO}_2\text{-PDA}\text{-}$ diatoms was analyzed by transepithelial electrical resistance (TEER) measurement. The collagen-based hydrogels described above were formed on insert part in transwell. RTgill-W1 cells cultured in BPA media or BPA treated with $\delta\text{-MnO}_2\text{-PDA}\text{-diatoms}$ media were planted on hydrogel surface with 200,000 cells cm $^{-2}$. The impedance of cells attached on hydrogel was measured by TEER measurement device (World precision instrument EVOM3) after 3 days culture (n = 3). The impedance data utilized for permeability of cells.

2.11. δ -MnO₂-PDA-diatom loaded packed column for continuous BPA degradation

A certain amount of δ -MnO₂-PDA-diatoms was loaded into a syringe and sealed with cotton and epoxy to assemble a customized packed column. The inlet was connected with a syringe pump (PHD ULTRATM) and the outlet was connected with a silicone tube for solution collection. The wastewater was obtained from Sanitary District of Decatur, IL (detailed composition in Table S4). The wastewater was collected before the disinfection stage, immediately after the clarifier step. The inlet BPA-spiked water and wastewater included 4.4 μ M BPA in acetate buffer (pH = 5) with 0.01 M NaCl. Before the treatment, the packed column was washed by pumping deionized water for 10 min. Then, to initiate the treatment, the BPA solution was introduced into the packed column with varying flow rates using a syringe pump. The treated solution was

collected at steady-state and the concentration of BPA was analyzed with HPLC as mentioned above.

2.12. Statistical analysis

The data were presented as mean \pm standard deviation unless otherwise specified, with three samples analyzed per condition. Oneway ANOVA followed by Turkey's post hoc analysis was performed for comparisons between groups to determine significance. Data were considered statistically significant with p values < 0.05.

3. Results and discussion

3.1. Synthesis and characterizations of δ -MnO₂-PDA-diatom

The δ -MnO₂-PDA-diatoms were fabricated by coating a layer of PDA binder on diatom biosilica particles and subsequently depositing δ -MnO₂ nanosheets (Scheme 1). Diatom biosilica particles are the skeleton of microalgae with porous structures. As shown in Fig. 1A-i, the diatom particle used in this study has a hollow, cylindrical shape with uniformly distributed 500 nm-diameter pores on the side. The particle size is $\sim 18~\mu m$ in length and $\sim 10~\mu m$ in diameter. The PDA layer formed through the polymerization of dopamine monomer on the diatom was confirmed with scanning and transmission electron microscopy (SEM and TEM) images. Compared to the smooth surface of the bare diatom (Fig. 1B-i), the resulting PDA-diatom showed rough surface due to the PDA layer (Fig. 1A-ii, 1B-ii). The TEM image also confirmed the PDA layer with a thickness of $\sim 50~nm$ (Fig. 1B-ii).

The resulting PDA layer served as a binder that activates *in situ* deposition of MnO_2 nanosheets on the diatom particles due to its intrinsic reducing ability as follows [49] (Equation (2)):

$$MnO_4^- + 2 H_2O + 3 e^- (from PDA) \rightarrow MnO_2 + 4 OH^-$$
 (2)

The electrons donated from the PDA layer reduced MnO₄ into MnO₂ in situ, forming MnO2 nanosheets on the PDA layer (Fig. 1A-iii). The element mapping images indicated that the formation of MnO2 nanosheets was uniformly distributed throughout the diatom particle (Fig. 1C). Furthermore, the TEM image (Fig. 1B-iii) revealed the twodimensional lamellar structure of the MnO_2 loaded on the PDA layer. The distances of lattice spacing were 0.36, 0.24, and 0.14 nm, corresponding to the (002), (111), and (020) planes of MnO₂ observed in the X-ray diffraction (XRD) pattern (Fig. 1D). In addition, the locations of peaks in the XRD pattern confirmed that the MnO2 nanosheets exclusively belonged to monoclinic birnessite (δ-MnO₂) [46,50,51]. The inductively coupled plasma-atomic emission spectroscopy (ICP-AES) measurement further confirmed that the Mn loading in the δ-MnO₂-PDA-diatoms was \sim 14.6 wt% (i.e., $\text{MnO}_2\sim$ 23 wt% based on stoichiometry). The X-ray photoelectron spectroscopy (XPS) analysis also indicated the existence of Mn(IV) (\sim 70.0%), Mn(III) (\sim 27.2%), and Mn (II) (\sim 2.8%) on the surface of diatom particles [38] (Fig. S1).

According to the nitrogen adsorption/desorption analysis, the curve of bare diatom particles was type IV isotherm with a hysteresis loop, characteristic of typical mesoporous structures (Fig. 1E). The BET surface area, pore volume, and pore diameter of bare diatom particles were $33.1 \text{ m}^2/\text{g}$, $0.113 \text{ cm}^3/\text{g}$, and 13.8 nm, respectively (Table S1). The hysteresis loop of PDA-diatom closed around $0.5 - 0.8\text{P/P}_0$ (Fig. 1E), indicating that the PDA binder layer blocked pores on the diatom partially. This analysis was also supported by the decreased BET surface area ($13.2 \text{ m}^2/\text{g}$) and pore volume ($0.058 \text{ cm}^3/\text{g}$). The slight increase in the pore size (18.2 nm) was attributed to the increased surface roughness with PDA coating [52] (Table S1 and Fig. 1A-ii). After the loading of δ-MnO₂, the hysteresis loop recurred and became even more significant than that of bare diatom due to the mesoporous structure of δ-MnO₂ nanosheets (Fig. 1B-iii, 1E). The substantial increase in BET surface area ($52.9 \text{ m}^2/\text{g}$) and pore volume ($0.092 \text{ cm}^3/\text{g}$), as well as the decrease in

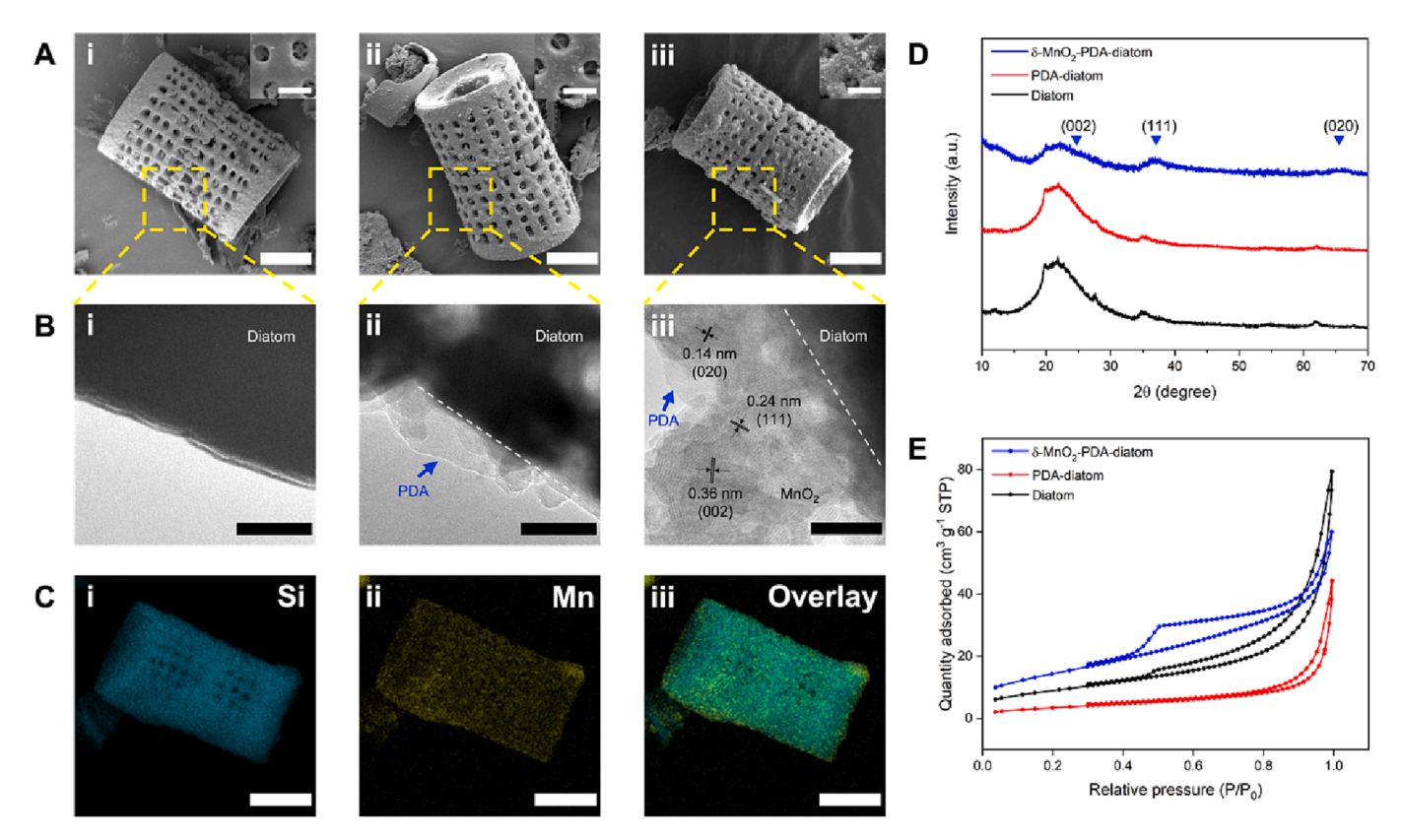


Fig. 1. Characterization of δ -MnO₂-PDA-diatom. (A) SEM images of (i) diatom, (ii) PDA-diatom, and (iii) δ -MnO₂-PDA-diatom. Scale bar: 5 μm. The inset images represent the corresponding image with higher magnification. Scale bar: 1 μm. (B) TEM images of (i) diatom, (ii) PDA-diatom, and (iii) δ -MnO₂-PDA-diatom. Scale bar: (i, ii)100 nm and (iii) 10 nm. The white dashed line represents the wall boundary of the diatom, and the blue arrow represents the location of the PDA layer. The black arrows represent the distance of lattice spacing. (C) Element mapping images of δ -MnO₂-PDA-diatom: (i) Si, (ii) Mn, and (iii) Overlay. Scale bar: 5 μm. (D) X-ray diffraction patterns and (E) nitrogen adsorption/desorption isotherms of diatom, PDA-diatom, and δ -MnO₂-PDA-diatom. (For interpretation of the references to color in this figure legend, the reader is referred to the web version of this article.)

pore diameter (7.3 nm), indicated the abundant existence of δ-MnO₂.

3.2. Kinetics of BPA degradation using δ -MnO₂-PDA-diatom

We examined the extent to which $\delta\text{-MnO}_2\text{-PDA-diatoms}$ degrade BPA at controlled rates in a batch reactor (Fig. 2A). Degradation of BPA with bare diatoms and PDA-diatoms were performed as control groups. According to Fig. 2A, BPA incubated with bare diatoms or PDA-diatoms kept their concentrations constant after a negligible drop, indicating that neither diatoms nor PDA degraded or adsorbed BPA molecules. In contrast, the BPA incubated with $\delta\text{-MnO}_2\text{-PDA-diatom}$ showed an exponential decrease in concentration over time. In particular, increasing the concentration of $\delta\text{-MnO}_2\text{-PDA-diatoms}$ from 0.1 to 1.0 g/L accelerated the BPA degradation, such that 99% of BPA was removed within 20 min. All the BPA degradation curves with varying concentrations of $\delta\text{-MnO}_2\text{-PDA-diatom}$ followed pseudo-first-order kinetics (Equation (3)):

$$\frac{[BPA]}{[BPA]_0} = e^{-kt} \tag{3}$$

where [BPA] is the concentration of BPA, [BPA] $_0$ is the initial concentration of BPA, k is the reaction rate constant, and t is the reaction time. The reaction rate constant for each concentration of δ -MnO $_2$ -PDA-diatoms was obtained by fitting the reaction curve with Equation (3) (Fig. S2). As shown in Fig. 2B and Table S2, the reaction rate constant was linearly proportional to the concentration of δ -MnO $_2$ -PDA-diatoms.

In general, the degradation of BPA is triggered by the electron transfer on the surface of MnO₂, which is believed to be the rate-determining step. Therefore, the linear dependence between the

reaction rate constant and concentration of δ-MnO₂-PDA-diatoms suggests that reactive sites of δ -MnO₂ on diatoms remain highly accessible for BPA degradation even with the increase of δ-MnO₂ concentration up to 1.0 g/L. The reaction rate constant based on the mass of δ-MnO₂-PDAdiatom was $0.178 \pm 0.002 \text{ L g}^{-1} \text{ min}^{-1}$, obtained from the slope in Fig. 2B. The net reaction rate constant based on the mass of δ-MnO₂ measured with ICP-AES was $0.774 \pm 0.009 \, \mathrm{L g^{-1} \, min^{-1}}$. Moreover, the reaction between BPA and δ-MnO₂ is still preferable with the presence of the competitive compound. When a compound also assembled with an aryl group, 2-chlorophenol, is mixed with BPA, there was no impact on the BPA degradation (Fig. S3). As shown in Fig. S3, BPA was degraded ~ 99% within 20 min while 2-chlorophenol was \sim 18% degradation with a selectivity of 5.56 (BPA/2-chlorophenol). Furthermore, the degradation of 2-chlorophenol continued (~57%) for the following 2 h with a selectivity of 1.79. These results further not only indicate the reactivity difference between the compounds with aryl group and δ-MnO₂, but also suggest the merit of highly accessible reactive sites of δ -MnO₂ on the surface of diatom particles for BPA removal.

Separately, free-standing $\delta\text{-MnO}_2$ was fabricated without diatom support through the sol–gel method [53]. The quantity of $\delta\text{-MnO}_2$ in the free-standing form and on the diatom particles was kept the same at 0.115 g/L for the BPA degradation test. The results showed that the BPA degradation by free-standing $\delta\text{-MnO}_2$ nearly followed pseudo-first-order kinetics (Fig. 2C and Fig. S4). However, the BPA degradation rate by free-standing $\delta\text{-MnO}_2$ was much lower than $\delta\text{-MnO}_2\text{-PDA}\text{-diatom}$. The reaction rate constant based on the mass of free-standing $\delta\text{-MnO}_2$ was 0.056 \pm 0.005 L g $^{-1}$ min $^{-1}$, \sim 14-fold lower than that of $\delta\text{-MnO}_2\text{-PDA}\text{-diatom}$ (Fig. 2D). This difference confirms the significant merits of immobilizing $\delta\text{-MnO}_2$ onto the micro-sized porous support, which

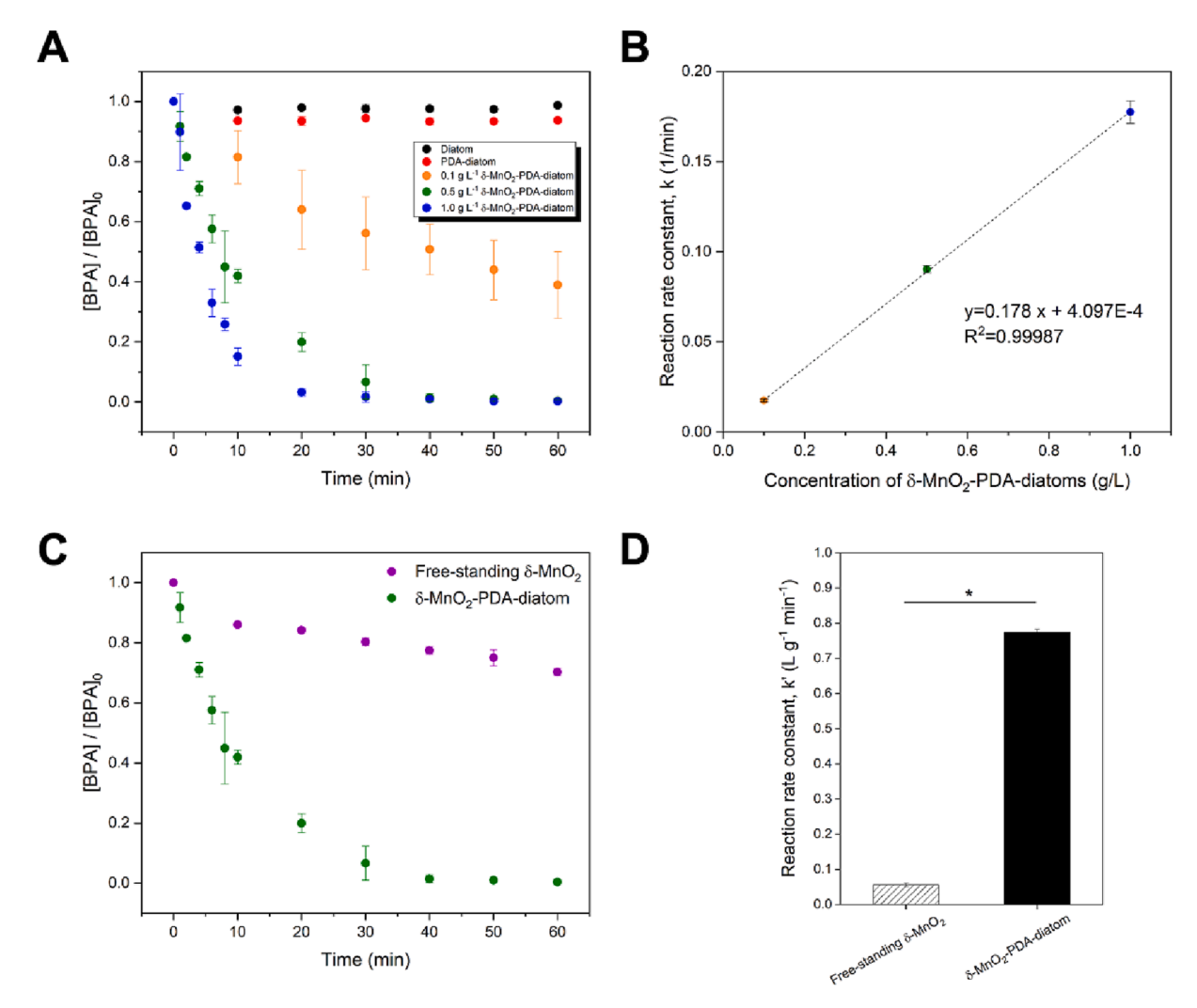


Fig. 2. Analysis of BPA degradation by δ -MnO₂-PDA-diatoms. (A) The dependency of BPA degradation rate on the concentration of δ -MnO₂-PDA-diatoms. [BPA]₀ = 4.4 μM, [NaCl] = 0.01 M, and pH = 5.0, n = 3. (B) The dependency of degradation rate constant (*k*) on the concentration of MnO₂-PDA-diatoms. (C) BPA degradation rates for free-standing δ -MnO₂ and δ -MnO₂-PDA-diatoms. The mass of δ -MnO₂ was fixed at 0.115 g/L for the two groups. [BPA]₀ = 4.4 μM, [NaCl] = 0.01 M, and pH = 5.0, n = 3. (D) Comparison of the reaction rate constant based on the net mass of δ -MnO₂ between free-standing δ -MnO₂ and δ -MnO₂-PDA-diatom. Bars represent the mean value, and error bars indicate the standard deviation. * represents a significant difference between the two groups. *p < 0.05 (n = 3).

increases the number of accessible active sites and also prevents catalysts from aggregation during the synthesis.

In addition, the $\delta\text{-MnO}_2$ immobilized on diatom particles through polydopamine coating demonstrates strong adhesion property which would further sustain its BPA degradation capability. As shown in Fig. S5, the BPA degradation was maintained at 99% removal rate after recycling $\delta\text{-MnO}_2\text{-PDA-diatoms}$ for at least 7 times. ICP-AES measurement also suggests that there was no Mn percentage change after the reaction with BPA, thus supporting its sustainability on BPA treatment without Mn leaching or reduction from the composite material. Taken together, these results indicate that the immobilization of $\delta\text{-MnO}_2$ on porous diatom particles not only can improve the reaction rate on BPA degradation but also can provide the reusability towards BPA removal in a sustainable and eco-friendly manner.

3.3. BPA degradation pathways with δ -MnO₂-PDA-diatoms

We studied the BPA degradation pathways activated by δ -MnO₂-PDA-diatoms. According to the LC-MS analysis, six products (I-VI) were identified after the degradation of BPA (Table S3, Figs. S6–S11). As shown in Fig. 3, we propose that product I shown in Fig. S6 is derived from the hydroxyl addition on the aromatic ring of BPA, which

subsequently forms monohydroxylated BPA in an aqueous environment (pathway a) [54]. In contrast, products II-VI identified in Figs. S7–S11 are mainly obtained from BPA degradation reaction on the surface of δ-MnO₂-PDA-diatoms (pathway **b**) [34]. It is proposed that BPA molecules are initially degraded to release radicals via electron transfer to the surface of MnO2. BPA radicals existed in four transition forms through radical resonance (radicals 1-4). Individual radicals likely trigger a series of coupling (pathway c) and fragmentation (pathway d) reactions to form intermediate compounds and products, as shown in Fig. S12. In pathway c, para C-O coupling of radical 1 and radical 2 is the most common reaction among radical coupling, producing cationic isopropylphenol as an intermediate compound [34]. The cationic isopropylphenol then triggers the substitution of water, ketonization, and deprotonation to yield products II (Fig. S7), III (Fig. S8), and IV (Fig. S9), respectively. In pathway d, the BPA radical 2 undergoes beta scission to release a phenoxy radical, which is later oxidized by MnO₂ to form product V (Fig. S10). At the same time, the cationic isopropylphenol can react with product V to generate product VI (Fig. S11) through substitution (pathway e) [34].

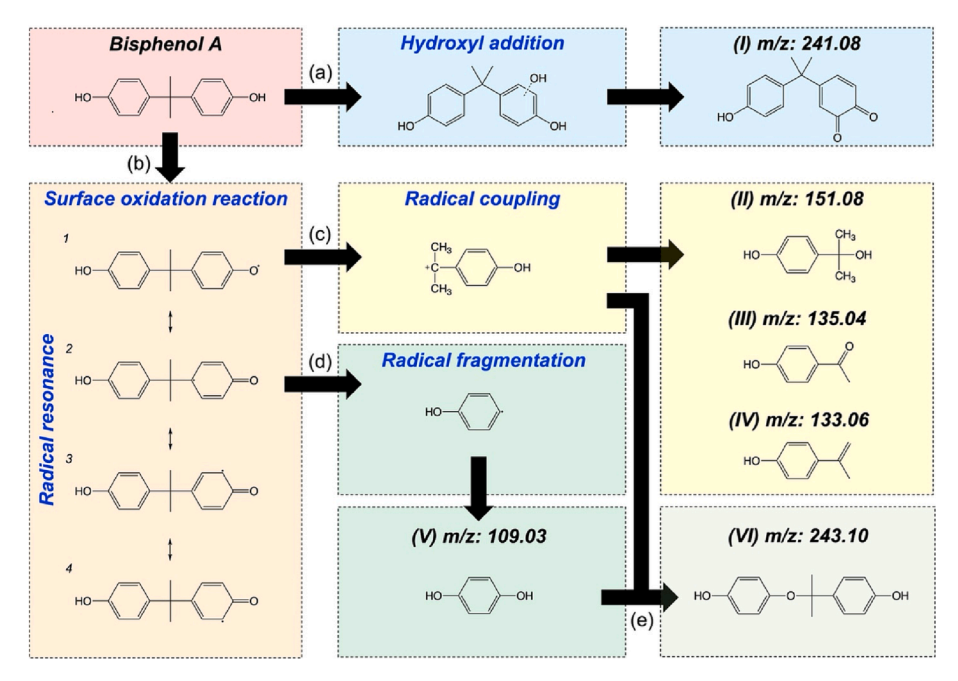


Fig. 3. δ -MnO₂-PDA-diatom-induced BPA degradation pathways determined by LC-MS analysis. Pathway (a) represents the hydroxyl addition on the BPA molecule. Pathway (b) shows the initial surface oxidation reaction of BPA molecules on δ -MnO₂-PDA-diatoms, followed by a series of BPA degradation processes: radical coupling (c), radical fragmentation (d), and cation substitution (e).

3.4. Evaluation of the extent to which δ -MnO₂-PDA-diatoms neutralize the estrogenic activity of BPA using human kidney cells

We assessed whether the δ-MnO₂-PDA-diatom decreases the

estrogenic activity of BPA as endocrine-disrupting chemicals (EDC). BPA is an environmental estrogen that can bind onto estrogen receptors (i.e., ER α and ER β) and disrupt cellular behaviors due to its similar molecular structure to endogenous estrogen, 17 β -estradiol (E2) [23,55]. For this

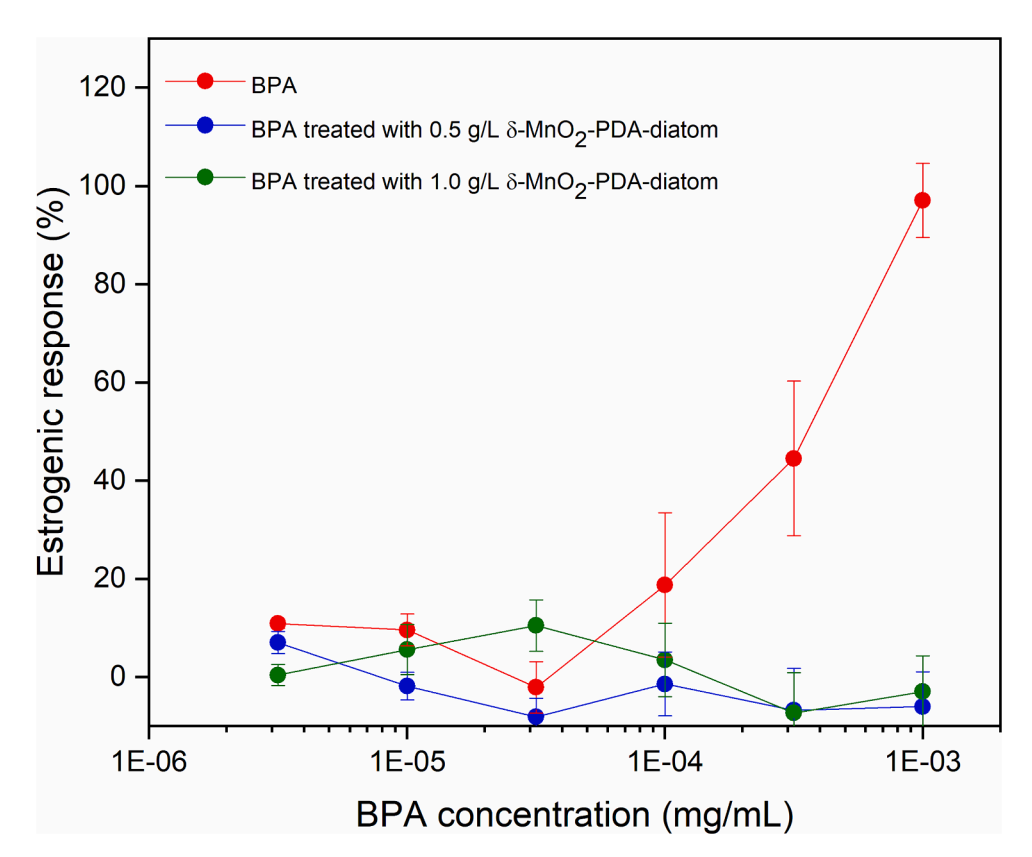


Fig. 4. The estrogenic activity of HKE293-ERE-zER α cells after exposure to BPA and BPA degraded by δ -MnO₂-PDA-diatoms for 20 min. Each solution was exposed to the cells for 24 h. The concentrations of δ -MnO₂-PDA-diatoms were 0.5 g/L or 1.0 g/L, respectively. The response value at 0.32 ng/mL of E2 was 100%. The data points represent the mean value, and the error bars indicate the standard deviation (n = 6).

study, human embryonic kidney 293 (HKE293) cells were engineered to carry estrogen response element (ERE) and zebrafish estrogen receptor alpha (zER α), termed HKE293-ERE-zER α cells. The resulting zER α could interact with estrogens, as confirmed by the positive response to E2 molecules. As shown in Fig. S13, the engineered HKE293-ERE-zER α cells exhibited a sigmoidal kinetic profile of estrogen response on the E2 concentration, indicating the positive, cooperative binding [56,57] between the E2 and the zER α .

As shown in Fig. 4, the cells incubated in the media contaminated by BPA showed a nearly sigmoidal kinetic dependency of estrogenic response on the BPA concentration. This kinetic profile indicated the positive and cooperative binding of BPA to the receptor zER α , like E2 in Fig. S13. Note that the range of the BPA concentration ($10^{-6}-10^{-3}$ mg mL $^{-1}$) is 1,000-fold higher than that of E2 concentration ($10^{-9}-10^{-6}$ mg mL $^{-1}$), corresponding to the previous finding that BPA has 1,000- to 2,000-fold lower affinity to the estrogenic receptors than E2 [58,59]. In contrast, the estrogenic response to BPA degraded by 0.5 or 1.0 g/L of δ -MnO₂-PDA-diatoms dropped to below 5% with initial BPA concentration across 10^{-6} to 10^{-3} mg mL $^{-1}$ after 24 h incubation. These results demonstrated that the degraded products derived from the reaction between BPA and δ -MnO₂-PDA-diatom are ineffective in activating the cellular estrogenic response, thus not acting as EDC any longer.

3.5. Evaluation of the extent that δ -MnO₂-PDA-diatoms reduce aquatic toxicity of BPA using rainbow trout gill cells

We further assessed the aquatic toxicity of BPA before and after treatments using δ -MnO₂-PDA-diatoms. This analysis used rainbow trout gill cells (RTgill-W1). Gill cells are sensitive to small chemical or physical changes due to their biological function for respiration and maintaining osmotic pressure. Therefore, gill cells have widely been used to evaluate the toxicity of industrial effluents (e.g., petroleum refinery and aromatic hydrocarbons) [60–63].

First, we examined the intracellular oxidative stress increased by overproduced reactive oxygen species (ROS). Cells were incubated with regular culture media, media contaminated by BPA, and media containing BPA treated with $\delta\text{-MnO}_2\text{-PDA-diatoms}$. The intracellular oxidative stress was examined with CellROX® Green reagent, which

binds to DNA localized around mitochondria and nucleus and generates a fluorescent signal upon oxidation [64].

As shown in Fig. 5A, cells incubated with regular culture media showed weak green fluorescence around the cell nucleus because of the endogenous ROS. In contrast, cells exposed to BPA displayed a nearly 3-fold higher fluorescent intensity around the nuclei (Fig. 5B). This result illustrates that BPA stimulates cellular ROS generation and, in turn, increases oxidative stress [64]. On the other hand, cells incubated with BPA degraded by $\delta\text{-MnO}_2\text{-PDA-diatoms}$ exhibited comparable fluorescence to cells incubated with regular culture media, indicating that products resulting from the BPA degradation minimally stimulate cellular ROS production.

Second, we assessed if degraded BPA products have harmful effects on tissue morphogenesis by examining the lamellar-shaped hollow lumen formation of RTgill-W1 cells. Gill cells in the regular culture media could reproduce the lamellar structure of fish gill on the hydrogel formed by a mixture of type I collagen, an essential extracellular matrix component, and polyethylene glycol (PEG) [48] (Fig. 6A-i and ii). However, the cells incubated in BPA-containing media exhibited minimal activities to form the hollow epithelial lumen. Conversely, cells incubated in media containing BPA degraded by $\delta\text{-MnO}_2\text{-PDA-diatoms}$ self-assembled into a filamentous hollow epithelial lumen, like cells not exposed to BPA.

In parallel, tissue morphogenesis of RTgill-W1 cells was evaluated by measuring transepithelial electrical resistance (TEER) [65]. This quantitative technique measures the integrity of the tight junction of epithelial cells in terms of impedance (Ω/cm^2). As shown in Fig. 6B, the impedance of untreated cells was $\sim 25~\Omega/cm^2$. In contrast, the impedance of cells incubated in the BPA-spiked media was reduced to $\sim 15~\Omega/cm^2$, due to the disintegrated intercellular junction observed in Fig. 6A. In contrast, the media containing BPA degraded by $\delta\text{-MnO}_2\text{-PDA-diatoms}$ minimally influenced the impedance of cells, as marked with $\sim 29~\Omega/cm^2$ similar to the impedance of untreated cells. These results prove that $\delta\text{-MnO}_2\text{-PDA-diatoms}$ can minimize the toxic effects of BPA on biological cells. The resulting degraded products are minimally toxic to cells, thus allowing cells to retain normal ROS levels and form tight intercellular junctions.

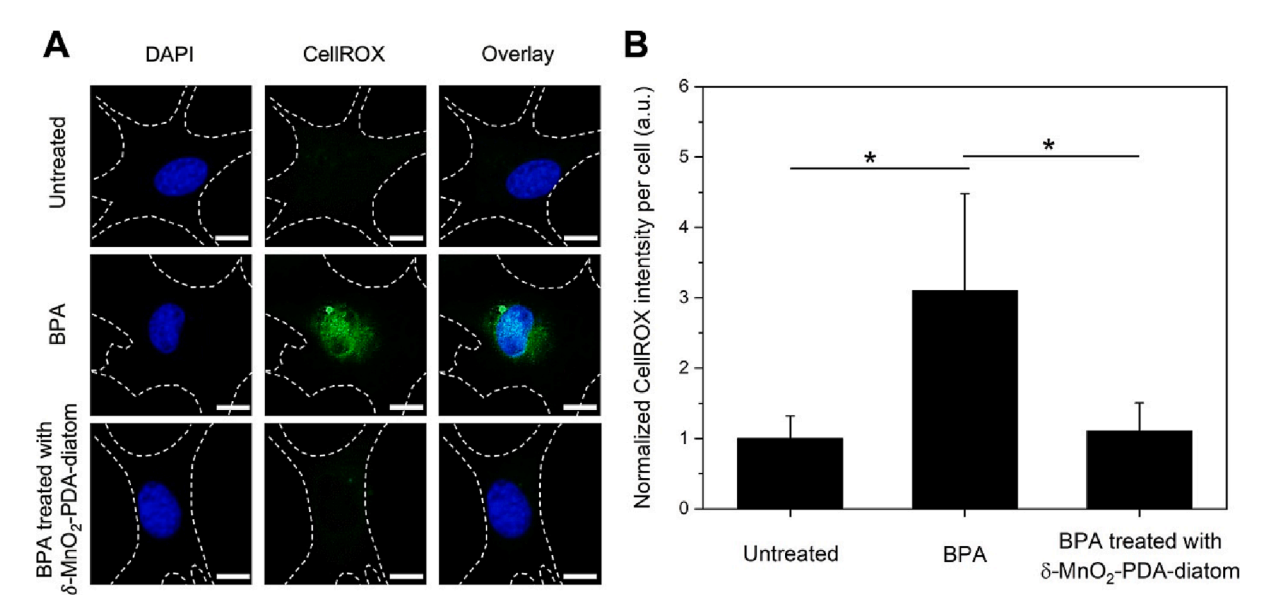


Fig. 5. Characterization of intracellular oxidative stress within rainbow trout gill (RTgill-W1) cells. (A) Representative confocal images of oxidative stress of RTgill-W1 cells incubated in the regular culture media (untreated, first row), media with BPA (second row), and media with BPA degraded by δ -MnO₂-PDA-diatom (third row). Blue color (DAPI) represents nuclei, and green color (CellROX®) represents the intracellular oxidative level. The white dashed lines represent the cell peripherals. Scale bar: 10 µm. (B) Normalized CellROX® intensity per gill cell incubated in the regular culture media (untreated), media with BPA, and media with BPA degraded by δ -MnO₂-PDA-diatoms. Bars represent the mean value, and error bars indicate the standard deviation. * represents significant difference between the two groups, *p < 0.05 (n = 10). (For interpretation of the references to color in this figure legend, the reader is referred to the web version of this article.)

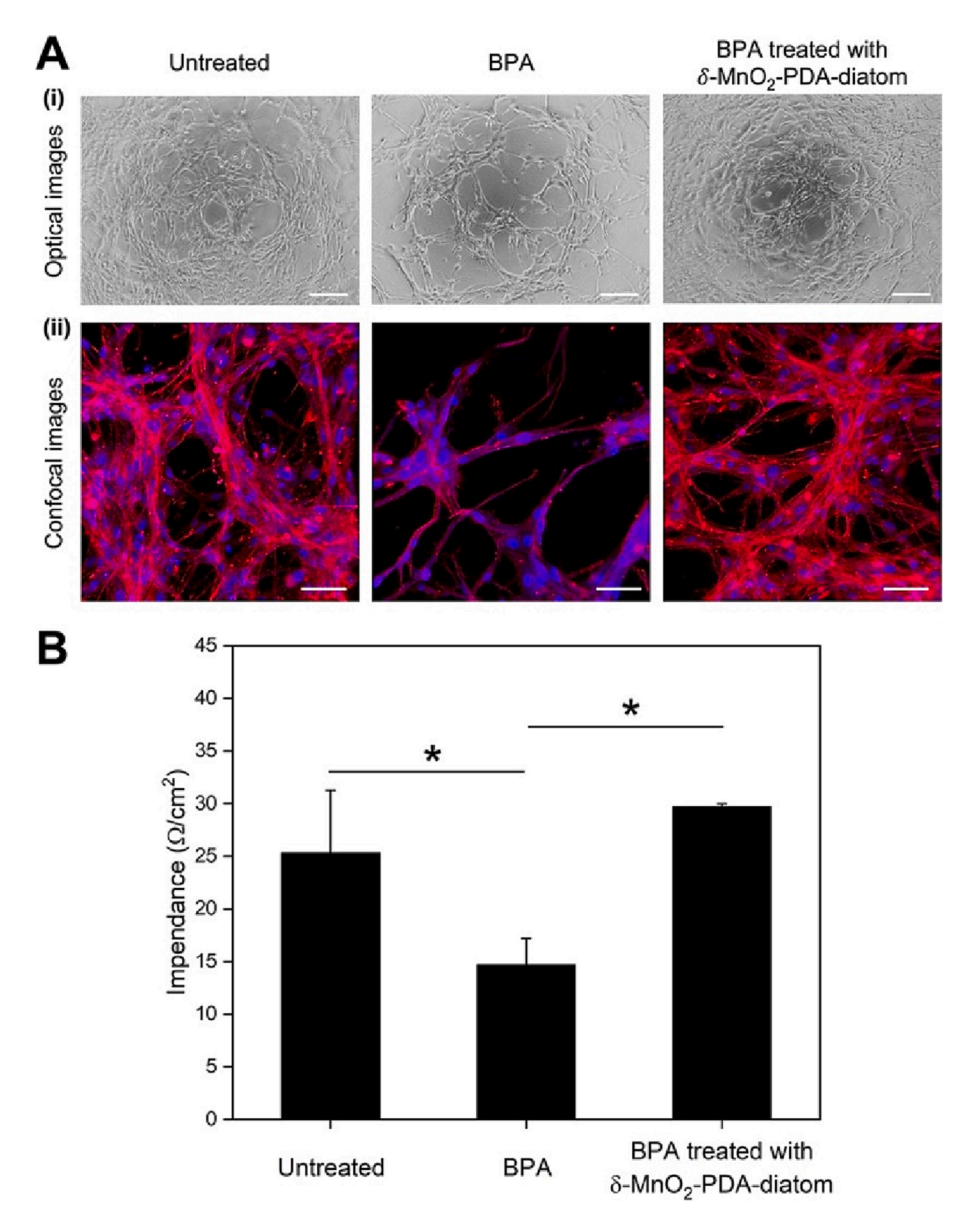


Fig. 6. Morphogenesis by RTgill-W1 cells exposed to BPA or BPA degraded by δ-MnO2-PDA-diatoms. (A) Analysis of the ability of gill cells to self-organize in the form of the hollow epithelial lumen: (i) optical images and (ii) confocal images. Blue represents nuclei stained with DAPI, and red represents F-actin labeled with Alex fluor 594. Scale bar: (i) 200 µm and (ii) 50 μm. (B) Transepithelial electrical resistance (TEER) measurement of the RTgill-W1 cells incubated in the regular culture media (untreated), media spiked with BPA, and media containing BPA degraded by $\delta\text{-MnO}_2\text{-PDA-diatoms}$. Bars represent the mean value, and error bars indicate the standard deviation. * represents significant difference between the two groups, *p < 0.05 (n = 3). (For interpretation of the references to color in this figure legend, the reader is referred to the web version of this article.)

3.6. δ -MnO₂-PDA-diatom loaded packed column for continuous BPA removal

We further tested the continuous BPA removal by packing a flow column with $\delta\text{-MnO}_2\text{-PDA-diatoms}.$ As shown in Fig. 7A, BPA-spiked water flowed steadily into the packed column at a flow rate up to 500 mL h^{-1} using a syringe pump. HPLC analysis of the outflow disclosed that $\delta\text{-MnO}_2\text{-PDA-diatoms}$ removed almost 99% of BPA (Fig. 7B). This result corresponds to the estimated conversion of BPA with pseudo-first-order kinetics in a packed column in Equation (4):

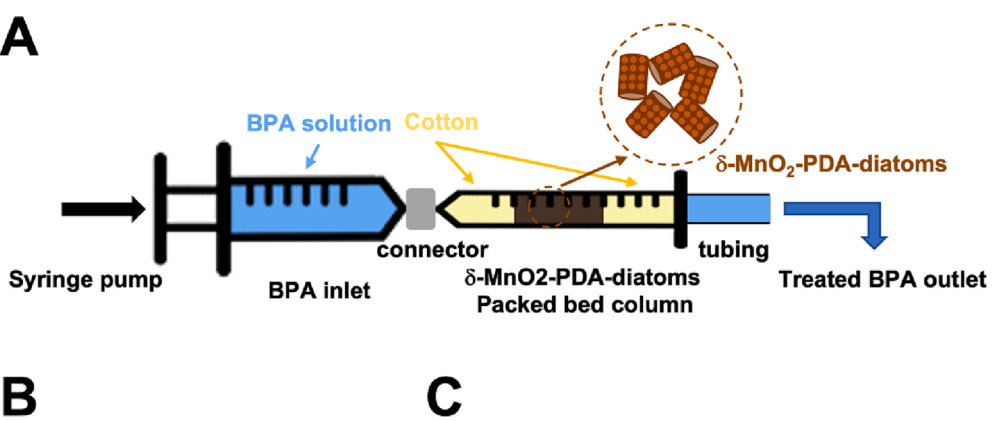
$$W = \frac{u_0}{k'} \int_0^X \frac{dX}{1 - X} \tag{4}$$

where W is the mass of δ-MnO₂, u_0 is the inlet flow rate, k' is the reaction rate constant based on the mass of δ-MnO₂, and X is the BPA conversion. As a control group, the BPA removal by pristine diatoms in a packed column only showed $\sim 10\%$ BPA removal, which might be attributed to the adsorption of BPA to the diatom particles (Fig. 7B). In addition, we further evaluated the BPA removal efficiency with varying inlet flow rates with BPA-spiked water (green) and wastewater (blue) (Fig. 7C). Both treatments suggested that a $\sim 99\%$ BPA removal was achieved, as

measured by HPLC analysis from 31.25 mL h^{-1} to 500 mL h^{-1} in a packed column, comparable with the theoretical calculation in Equation (4). These results demonstrate a proof-of-concept to continuously degrade BPA-spiked water with high efficiency and effectiveness, illuminating an advanced large-scale cleaning strategy.

4. Conclusions

This study demonstrates that immobilizing $\delta\textsc{-MnO}_2$ nanosheets onto porous diatom silica particles is advantageous to neutralizing BPA in water for both batch and continuous processes. Polydopamine-coated diatoms enabled in situ immobilization of MnO2 precursors to form nanosheets on the diatom surface. The resulting $\delta\textsc{-MnO}_2\textsc{-PDA}\textsc{-diatom}$ degraded more than 99 % of BPA in a water container within 20 min by following pseudo-first-order kinetics (k' $\sim\!0.774\,L\,g^{-1}\,min^{-1}$). Increased BPA degradation rate with the mass of $\delta\textsc{-MnO}_2\textsc{-PDA}\textsc{-diatom}$ indicates the crucial role of diatoms in presenting active sites of $\delta\textsc{-MnO}_2$ while preventing aggregation. Therefore, the degradation rate constant of $\delta\textsc{-MnO}_2\textsc{-PDA}\textsc{-diatom}$ is $\sim 14\textsc{-fold}$ higher than free-standing $\delta\textsc{-MnO}_2$ nanosheets. Moreover, $\delta\textsc{-MnO}_2\textsc{-PDA}\textsc{-diatom}$ can be recycled without any performance lose on BPA degradation up to 7 times, which provides



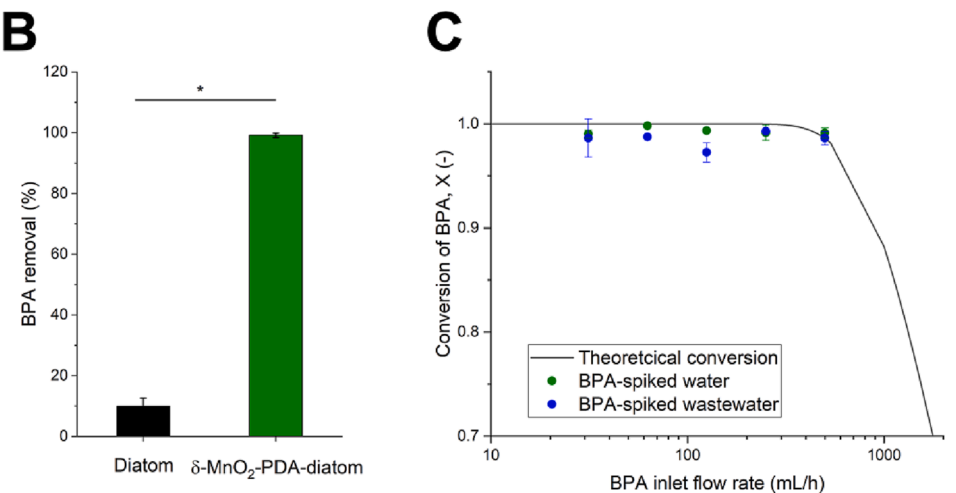


Fig. 7. Continuous BPA removal system by installing δ-MnO2-PDA-diatoms in a packed bed column. (A) Set-up of continuous flow coupled with a column loaded with δ-MnO₂-PDA-diatoms. Aqueous BPA solution was injected into the δ-MnO₂-PDA-diatomspacked bed column at controlled flow rates using a syringe pump. The BPA solution flowing through the outlet was analyzed with HPLC. (B) The BPA removal efficacy after the continuous treatment within a packed bed column. The density of δ-MnO₂-PDA-diatoms in the packed bed column was 0.5 g cm^{-3} . [BPA]₀ = 4.4 µM. [NaCl] = 0.01~M, and pH=5.0. Bars represent the mean value, and error bars indicate the standard deviation. * represents significant difference between the two groups, *p < 0.05 (n = 3). (C) The dependency of BPA removal efficacy on the BPA solution flow rate at inlets. The curve is theoretical conversion of BPA obtained from Equation (4). The green and blue data points represent the mean value of the conversion of BPA with BPA-spiked water and wastewater respectively. The error bars indicate the standard deviation (n = 3). (For interpretation of the references to color in this figure legend, the reader is referred to the web version of this

the reusability towards BPA removal in a sustainable and eco-friendly manner. Degraded products resulting from a series of radical transfers, coupling, and fragmentation reactions do not cause any estrogenic response or toxicity as examined with s human kidney cell and a trout gill cell. Therefore, $\delta\text{-MnO}_2\text{-PDA-diatom}$ serves to retain normal oxidative stress levels and tissue morphogenesis of cells exposed to the BPA-spiked water. The column packed with $\delta\text{-MnO}_2\text{-PDA-diatom}$ further shows ~ 99 % BPA removal in a continuous flow. Hence, the $\delta\text{-MnO}_2\text{-PDA-diatom}$ materials was shown to be a highly promising platform for the quick and reliable treatment of BPA-impacted water. The results offer a promising strategy for an efficient and effective path to clean various endocrine-disrupting chemicals that will disrupt physiological function of individual organs and cross-talks.

Declaration of Competing Interest

The authors declare that they have no known competing financial interests or personal relationships that could have appeared to influence the work reported in this paper.

Data availability

Data will be made available on request.

Acknowledgments

H.K. appreciate the National Science Foundation (NSF-DMR 2004719) and the SerVaas Lab for financial support. X.S. would like to thank a funding from the National Science Foundation (NSF CBET Grant #1942971). Y.K. would like to thank the funding from KIST-Europe (NRF-2017M3A7B6052455). Nitrogen adsorption/desorption, BET surface area, and ICP-AES measurements were conducted at the Microanalysis Laboratory (SCS CORES) at the University of Illinois. XRD was

conducted at the George L. Clark X-Ray Facility and 3M Materials Laboratory (SCS CORES) at the University of Illinois. SEM, TEM, and XPS analyses were performed at the Frederick Seitz Materials Research Laboratory Central Facilities at the University of Illinois. Laser scanning confocal microscopy imaging was conducted at the Core Facilities at the Carl R. Woese Institute for Genomic Biology at the University of Illinois.

Appendix A. Supplementary data

Supplementary data to this article can be found online at https://doi.org/10.1016/j.cej.2023.144653.

References

- F.-L. Jin, X. Li, S.-J. Park, Synthesis and application of epoxy resins: A review, J. Ind. Eng. Chem. 29 (2015) 1–11, https://doi.org/10.1016/j.jiec.2015.03.026.
- [2] B. Bae, J.H. Jeong, S.J. Lee, The quantification and characterization of endocrine disruptor bisphenol-A leaching from epoxy resin, Water Sci. Technol. 46 (2002) 381–387, https://doi.org/10.2166/wst.2002.0766.
- [3] K.P. Unnikrishnan, E.T. Thachil, Toughening of epoxy resins, Des. Monomers Polym. 9 (2006) 129–152, https://doi.org/10.1163/156855506776382664.
- [4] J.L. Carwile, H.T. Luu, L.S. Bassett, D.A. Driscoll, C. Yuan, J.Y. Chang, X. Ye, A. M. Calafat, K.B. Michels, Polycarbonate bottle use and urinary bisphenol A concentrations, Environ. Health Perspect. 117 (9) (2009) 1368–1372.
- [5] E.J. Hoekstra, C. Simoneau, Release of bisphenol A from polycarbonate—a review, Crit. Rev. Food Sci. Nutr. 53 (2013) 386–402, https://doi.org/10.1080/ 10408398.2010.536919.
- [6] K.L. Howdeshell, P.H. Peterman, B.M. Judy, J.A. Taylor, C.E. Orazio, R.L. Ruhlen, F.S. Vom Saal, W.V. Welshons, Bisphenol A is released from used polycarbonate animal cages into water at room temperature, Environ. Health Perspect. 111 (9) (2003) 1180–1187.
- [7] J. Sajiki, J. Yonekubo, Leaching of bisphenol A (BPA) from polycarbonate plastic to water containing amino acids and its degradation by radical oxygen species, Chemosphere 55 (2004) 861–867, https://doi.org/10.1016/j. chemosphere.2003.11.065.
- [8] S. Almeida, A. Raposo, M. Almeida-González, C. Carrascosa, Bisphenol A: food exposure and impact on human health, Compr. Rev. Food Sci. Food Saf. 17 (2018) 1503–1517, https://doi.org/10.1111/1541-4337.12388.

- [9] T. Geens, D. Aerts, C. Berthot, J.-P. Bourguignon, L. Goeyens, P. Lecomte, G. Maghuin-Rogister, A.-M. Pironnet, L. Pussemier, M.-L. Scippo, J. van Loco, A. Covaci, A review of dietary and non-dietary exposure to bisphenol-A, Food Chem. Toxicol. 50 (2012) 3725–3740, https://doi.org/10.1016/j.fct.2012.07.059.
- [10] M. Lorber, A. Schecter, O. Paepke, W. Shropshire, K. Christensen, L. Birnbaum, Exposure assessment of adult intake of bisphenol A (BPA) with emphasis on canned food dietary exposures, Environ. Int. 77 (2015) 55–62, https://doi.org/10.1016/j. envint.2015.01.008.
- [11] Y. Hu, Q. Zhu, X. Yan, C. Liao, G. Jiang, Occurrence, fate and risk assessment of BPA and its substituents in wastewater treatment plant: A review, Environ. Res. 178 (2019), 108732, https://doi.org/10.1016/j.envres.2019.108732.
- [12] M. Umar, F. Roddick, L. Fan, H.A. Aziz, Application of ozone for the removal of bisphenol A from water and wastewater – A review, Chemosphere 90 (2013) 2197–2207, https://doi.org/10.1016/j.chemosphere.2012.09.090.
- [13] H.-B. Lee, T.E. Peart, Bisphenol A contamination in Canadian municipal and industrial wastewater and sludge samples, Water Quality Res. J. 35 (2000) 283–298, https://doi.org/10.2166/wqrj.2000.018.
- [14] D.P. Mohapatra, S.K. Brar, R.D. Tyagi, R.Y. Surampalli, Occurrence of bisphenol A in wastewater and wastewater sludge of CUQ treatment plant, J. Xenobiot. 1 (2011) 63
- [15] M.S. Muhamad, M.R. Salim, W.J. Lau, Z. Yusop, A review on bisphenol A occurrences, health effects and treatment process via membrane technology for drinking water, Environ. Sci. Pollution Res. 23 (2016) 11549–11567, https://doi.org/10.1007/s11356-016-6357-2.
- [16] S.Y. Wee, A.Z. Aris, Endocrine disrupting compounds in drinking water supply system and human health risk implication, Environ. Int. 106 (2017) 207–233, https://doi.org/10.1016/j.envint.2017.05.004.
- [17] M.F. Rahman, E.K. Yanful, S.Y. Jasim, Endocrine disrupting compounds (EDCs) and pharmaceuticals and personal care products (PPCPs) in the aquatic environment: implications for the drinking water industry and global environmental health, J. Water Health 7 (2009) 224–243, https://doi.org/10.2166/wh.2009.021.
- [18] C.C. Willhite, G.L. Ball, C.J. McLellan, Derivation of a Bisphenol A Oral Reference Dose (RfD) and drinking-water equivalent concentration, J. Toxicol. Environ. Health Part B 11 (2008) 69–146, https://doi.org/10.1080/10937400701724303.
- [19] R. Huang, Z. Liu, S. Yuan, H. Yin, Z. Dang, P. Wu, Worldwide human daily intakes of bisphenol A (BPA) estimated from global urinary concentration data (2000–2016) and its risk analysis, Environ. Pollut. 230 (2017) 143–152, https:// doi.org/10.1016/j.envpol.2017.06.026.
- [20] Y. Ma, H. Liu, J. Wu, L. Yuan, Y. Wang, X. Du, R. Wang, P.W. Marwa, P. Petlulu, X. Chen, H. Zhang, The adverse health effects of bisphenol A and related toxicity mechanisms, Environ. Res. 176 (2019), 108575, https://doi.org/10.1016/j.envres.2019.108575.
- [21] F. Acconcia, V. Pallottini, M. Marino, Molecular mechanisms of action of BPA, Dose-Response 13 (2015), 1559325815610582, https://doi.org/10.1177/ 1559325815610582.
- [22] B.S. Rubin, Bisphenol A: An endocrine disruptor with widespread exposure and multiple effects, J. Steroid Biochem. Mol. Biol. 127 (2011) 27–34, https://doi.org/ 10.1016/j.jsbmb.2011.05.002.
- [23] I. Ďurovcová, S. Kyzek, J. Fabová, J. Makuková, E. Gálová, A. Ševčovičová, Genotoxic potential of bisphenol A: A review, Environ. Pollut. 306 (2022), 119346, https://doi.org/10.1016/j.envpol.2022.119346.
- [24] S. Hube, M. Eskafi, K.F. Hrafnkelsdóttir, B. Bjarnadóttir, M.Á. Bjarnadóttir, S. Axelsdóttir, B. Wu, Direct membrane filtration for wastewater treatment and resource recovery: A review, Sci. Total Environ. 710 (2020), 136375, https://doi. org/10.1016/j.scitotenv.2019.136375.
- [25] Y. Zhang, C. Causserand, P. Aimar, J.P. Cravedi, Removal of bisphenol A by a nanofiltration membrane in view of drinking water production, Water Res. 40 (2006) 3793–3799, https://doi.org/10.1016/j.watres.2006.09.011.
- [26] S.P. Dharupaneedi, S.K. Nataraj, M. Nadagouda, K.R. Reddy, S.S. Shukla, T. M. Aminabhavi, Membrane-based separation of potential emerging pollutants, Sep. Purif. Technol. 210 (2019) 850–866, https://doi.org/10.1016/j.seppur.2018.09.003.
- [27] E.M. Rodríguez, G. Fernández, N. Klamerth, M.I. Maldonado, P.M. Álvarez, S. Malato, Efficiency of different solar advanced oxidation processes on the oxidation of bisphenol A in water, Appl. Catal. B 95 (2010) 228–237, https://doi. org/10.1016/j.apcatb.2009.12.027.
- [28] I. Gültekin, N.H. Ince, Synthetic endocrine disruptors in the environment and water remediation by advanced oxidation processes, J. Environ. Manage. 85 (2007) 816–832, https://doi.org/10.1016/j.jenvman.2007.07.020.
- [29] S. Esplugas, D.M. Bila, L.G.T. Krause, M. Dezotti, Ozonation and advanced oxidation technologies to remove endocrine disrupting chemicals (EDCs) and pharmaceuticals and personal care products (PPCPs) in water effluents, J. Hazard. Mater. 149 (2007) 631–642, https://doi.org/10.1016/j.jhazmat.2007.07.073.
- [30] W. Zhang, K. Yin, L. Chen, Bacteria-mediated bisphenol A degradation, Appl. Microbiol. Biotechnol. 97 (2013) 5681–5689, https://doi.org/10.1007/s00253-013.4040.7
- [31] C. Zhang, Y. Li, C. Wang, L. Niu, W. Cai, Occurrence of endocrine disrupting compounds in aqueous environment and their bacterial degradation: A review, Crit. Rev. Environ. Sci. Technol. 46 (2016) 1–59, https://doi.org/10.1080/ 10643389.2015.1061881.
- [32] J.-H. Kang, Y. Katayama, F. Kondo, Biodegradation or metabolism of bisphenol A: From microorganisms to mammals, Toxicology 217 (2006) 81–90, https://doi.org/ 10.1016/j.tox.2005.10.001.

- [33] C.B. Godiya, B.J. Park, Removal of bisphenol A from wastewater by physical, chemical and biological remediation techniques. A review, Environ. Chem. Lett. 20 (2022) 1801–1837, https://doi.org/10.1007/s10311-021-01378-6.
- [34] K. Lin, W. Liu, J. Gan, Oxidative removal of Bisphenol A by manganese dioxide: efficacy, products, and pathways, Environ. Sci. Tech. 43 (2009) 3860–3864, https://doi.org/10.1021/es900235f.
- [35] C.K. Remucal, M. Ginder-Vogel, A critical review of the reactivity of manganese oxides with organic contaminants, Environ. Sci. Process Impacts 16 (2014) 1247–1266, https://doi.org/10.1039/C3EM00703K.
- [36] X. Tan, Y. Wan, Y. Huang, C. He, Z. Zhang, Z. He, L. Hu, J. Zeng, D. Shu, Three-dimensional MnO2 porous hollow microspheres for enhanced activity as ozonation catalysts in degradation of bisphenol A, J. Hazard. Mater. 321 (2017) 162–172, https://doi.org/10.1016/j.jhazmat.2016.09.013.
- [37] J. Huang, S. Zhong, Y. Dai, C.-C. Liu, H. Zhang, Effect of MnO2 phase structure on the oxidative reactivity toward bisphenol A degradation, Environ. Sci. Tech. 52 (2018) 11309–11318, https://doi.org/10.1021/acs.est.8b03383.
- [38] J. Huang, Y. Dai, K. Singewald, C.-C. Liu, S. Saxena, H. Zhang, Effects of MnO2 of different structures on activation of peroxymonosulfate for bisphenol A degradation under acidic conditions, Chem. Eng. J. 370 (2019) 906–915, https:// doi.org/10.1016/j.cej.2019.03.238.
- [39] E. Saputra, S. Muhammad, H. Sun, H.M. Ang, M.O. Tadé, S. Wang, Different crystallographic one-dimensional MnO2 nanomaterials and their superior performance in catalytic phenol degradation, Environ. Sci. Tech. 47 (2013) 5882–5887, https://doi.org/10.1021/es400878c.
- [40] P.S. Nico, R.J. Zasoski, Importance of Mn(III) availability on the rate of Cr(III) oxidation on δ-MnO2, Environ. Sci. Tech. 34 (2000) 3363–3367, https://doi.org/10.1021/es991462j.
- [41] P.S. Nico, R.J. Zasoski, Mn(III) center availability as a rate controlling factor in the oxidation of phenol and sulfide on δ-MnO2, Environ. Sci. Tech. 35 (2001) 3338–3343, https://doi.org/10.1021/es001848q.
- [42] U. Maitra, B.S. Naidu, A. Govindaraj, C.N.R. Rao, Importance of trivalency and the e g1 configuration in the photocatalytic oxidation of water by Mn and Co oxides, PNAS 110 (29) (2013) 11704–11707.
- [43] P. Munnik, P.E. de Jongh, K.P. de Jong, Recent developments in the synthesis of supported catalysts, Chem. Rev. 115 (2015) 6687–6718, https://doi.org/10.1021/ cr500486u.
- [44] A. Schätz, O. Reiser, W.J. Stark, Nanoparticles as semi-heterogeneous catalyst supports, Chem. Eur. J. 16 (2010) 8950–8967, https://doi.org/10.1002/ chem.200903462.
- [45] D.J. Cole-Hamilton, R.P. Tooze, eds., Catalyst Separation, Recovery and Recycling, Springer. 2006.
- [46] J. Yan, L. Yang, M.-F. Lin, J. Ma, X. Lu, P.S. Lee, Polydopamine spheres as active templates for convenient synthesis of various nanostructures, Small 9 (2013) 596–603, https://doi.org/10.1002/smll.201201064.
- [47] A.R. Mendenhall, P.M. Tedesco, L.D. Taylor, A. Lowe, J.R. Cypser, T.E. Johnson, Expression of a single-copy hsp-16.2 reporter predicts life span, J. Gerontol. Ser. A 67 (2012) 726–733, https://doi.org/10.1093/gerona/glr225.
- [48] K.M. Sullivan, C.G. Park, J.D. Ito, M. Kandel, G. Popescu, Y.J. Kim, H. Kong, Matrix softness-mediated 3D Zebrafish hepatocyte modulates response to endocrine disrupting chemicals, Environ. Sci. Technol. 54 (2020) 13797–13806, https://doi. org/10.1021/acs.est.0c01988.
- [49] Y. Li, R. Zhao, S. Chao, B. Sun, C. Wang, X. Li, Polydopamine coating assisted synthesis of MnO2 loaded inorganic/organic composite electrospun fiber adsorbent for efficient removal of Pb2+ from water, Chem. Eng. J. 344 (2018) 277–289, https://doi.org/10.1016/j.cej.2018.03.044.
- [50] K. Cao, H. Liu, Y. Li, Y. Wang, L. Jiao, Encapsulating sulfur in δ-MnO2 at room temperature for Li-S battery cathode, Energy Storage Mater. 9 (2017) 78–84, https://doi.org/10.1016/j.ensm.2017.06.012.
- [51] J.M.d.O. Cremonezzi, D.Y. Tiba, S.H. Domingues, Fast synthesis of δ-MnO2 for a high-performance supercapacitor electrode, SN Appl. Sci. 2 (10) (2020), https:// doi.org/10.1007/s42452-020-03488-2.
- [52] Y. Gao, X. Sang, Y. Chen, Y. Li, B. Liu, J. Sheng, Y. Feng, L. Li, H. Liu, X. Wang, C. Kuang, Y. Zhai, Polydopamine modification electrospun polyacrylonitrile fibrous membrane with decreased pore size and dendrite mitigation for lithium ion battery, J. Mater. Sci. 55 (2020) 3549–3560, https://doi.org/10.1007/s10853-019.04218.0
- [53] T. Uematsu, Y. Miyamoto, Y. Ogasawara, K. Suzuki, K. Yamaguchi, N. Mizuno, Molybdenum-doped a-MnO2 as an efficient reusable heterogeneous catalyst for aerobic sulfide oxygenation, Catal. Sci. Technol. 6 (2016) 222–233, https://doi. org/10.1039/C5CY01552A.
- [54] L. Wang, J. Jiang, S.-Y. Pang, Y. Zhou, J. Li, S. Sun, Y. Gao, C. Jiang, Oxidation of bisphenol A by nonradical activation of peroxymonosulfate in the presence of amorphous manganese dioxide, Chem. Eng. J. 352 (2018) 1004–1013, https://doi. org/10.1016/j.cei.2018.07.103.
- [55] R.K. Bhandari, S.L. Deem, D.K. Holliday, C.M. Jandegian, C.D. Kassotis, S.C. Nagel, D.E. Tillitt, F.S. vom Saal, C.S. Rosenfeld, Effects of the environmental estrogenic contaminants bisphenol A and 17α-ethinyl estradiol on sexual development and adult behaviors in aquatic wildlife species, Gen. Comp. Endocrinol. 214 (2015) 195–219, https://doi.org/10.1016/j.ygcen.2014.09.014.
- [56] M. Shou, Q. Mei, J.R.M.W. Ettore, R. Dai, T.A. Baillie, T.H. Rushmore, Sigmoidal kinetic model for two co-operative substrate-binding sites in a cytochrome P450 3A4 active site: an example of the metabolism of diazepam and its derivatives, Biochem. J. 340 (1999) 845–853, https://doi.org/10.1042/bj3400845.
- [57] F. Bontemps, L. Hue, H.-G. Hers, Phosphorylation of glucose in isolated rat hepatocytes. Sigmoidal kinetics explained by the activity of glucokinase alone, Biochem. J. 174 (1978) 603–611, https://doi.org/10.1042/bj1740603.

- [58] A. Bolli, P. Galluzzo, P. Ascenzi, G. del Pozzo, I. Manco, M.T. Vietri, L. Mita, L. Altucci, D.G. Mita, M. Marino, Laccase treatment impairs bisphenol A-induced cancer cell proliferation affecting estrogen receptor α-dependent rapid signals, IUBMB Life 60 (2008) 843–852, https://doi.org/10.1002/iub.130.
- [59] A. Bolli, P. Bulzomi, P. Galluzzo, F. Acconcia, M. Marino, Bisphenol A impairs estradiol-induced protective effects against DLD-1 colon cancer cell growth, IUBMB Life 62 (2010) 684–687, https://doi.org/10.1002/iub.370.
- [60] V.R. Dayeh, K. Schirmer, N.C. Bols, Applying whole-water samples directly to fish cell cultures in order to evaluate the toxicity of industrial effluent, Water Res. 36 (2002) 3727–3738, https://doi.org/10.1016/S0043-1354(02)00078-7.
- [61] K. Schirmer, D.J. Tom, N.C. Bols, J.P. Sherry, Ability of fractionated petroleum refinery effluent to elicit cyto- and photocytotoxic responses and to induce 7ethoxyresorufin-O-deethylase activity in fish cell lines, Sci. Total Environ. 271 (2001) 61–78, https://doi.org/10.1016/S0048-9697(00)00831-7.
- [62] K. Schirmer, D.G. Dixon, B.M. Greenberg, N.C. Bols, Ability of 16 priority PAHs to be directly cytotoxic to a cell line from the rainbow trout gill, Toxicology 127 (1998) 129–141, https://doi.org/10.1016/S0300-483X(98)00030-4.
- [63] K. Schirmer, J.-A.-S. Herbrick, B.M. Greenberg, D.G. Dixon, N.C. Bols, Use of fish gill cells in culture to evaluate the cytotoxicity and photocytotoxicity of intact and photomodified creosote, Environ. Toxicol. Chem. 18 (1999) 1277–1288, https:// doi.org/10.1002/etc.5620180630.
- [64] R. Miller, Y. Kim, C.G. Park, C. Torres, B. Kim, J. Lee, D. Flaherty, H.-S. Han, Y. J. Kim, H. Kong, Extending the bioavailability of hydrophilic antioxidants for metal ion detoxification via crystallization with polysaccharide dopamine, ACS Appl. Mater. Interfaces 14 (2022) 39759–39774, https://doi.org/10.1021/
- [65] S. Chen, R. Einspanier, J. Schoen, Transepithelial electrical resistance (TEER): a functional parameter to monitor the quality of oviduct epithelial cells cultured on filter supports, Histochem. Cell Biol. 144 (2015) 509–515, https://doi.org/ 10.1007/s00418-015-1351-1.